# METAUX - ORGANIQUES

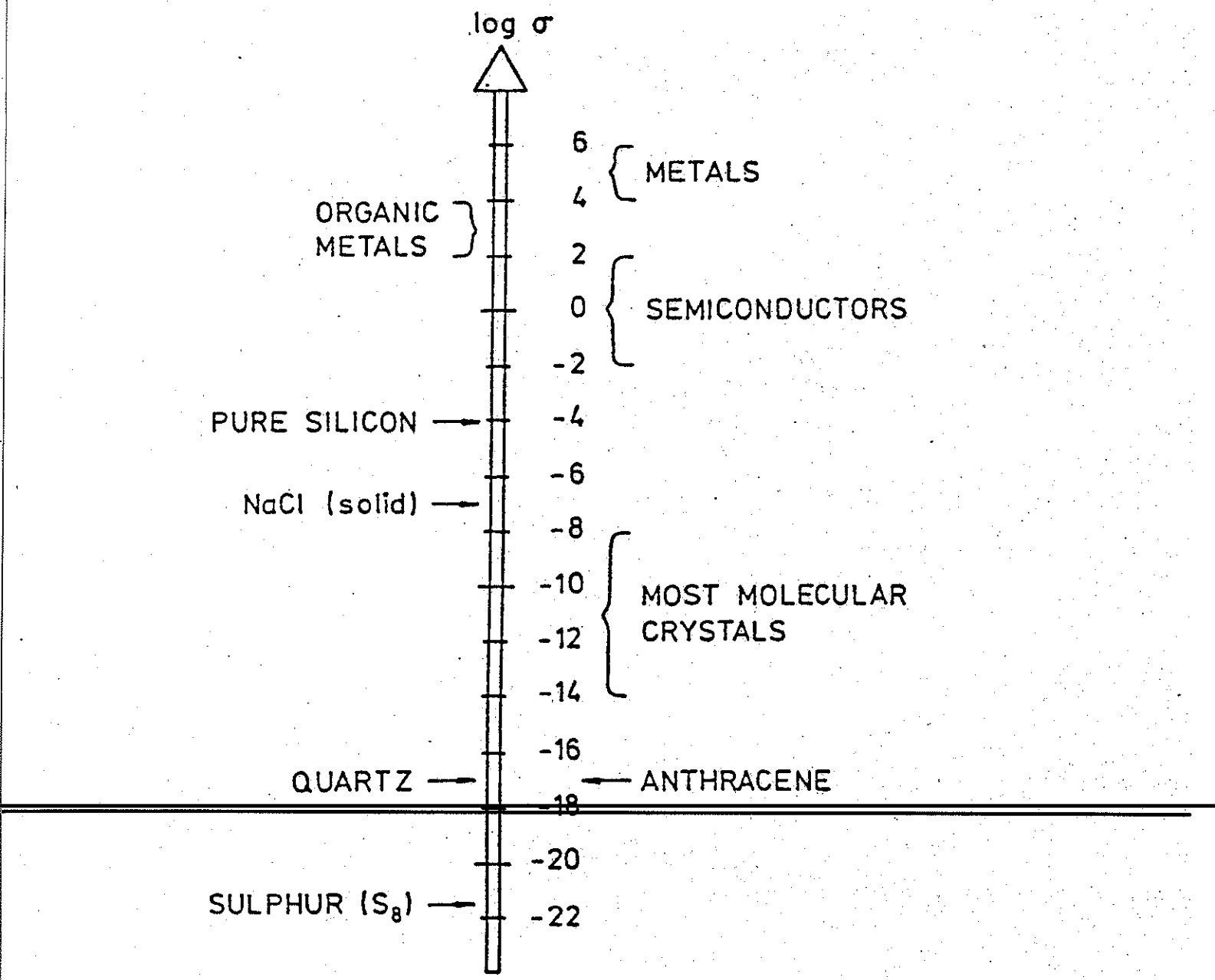


Scale of approximate conductivities at room-temperature for some selected materials.

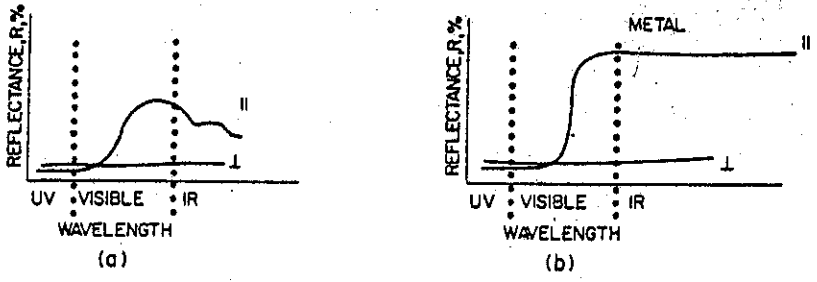


FIGURE 4. Schematic illustration of the frequency dependence of the reflectivity for a metal (b) and a highly reflecting nonmetal (a).

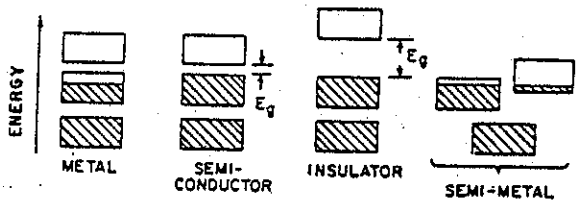


FIGURE 6. Schematic illustration of the electronic structure of a metal, semiconductor, and insulator with a gap, $E_g$, and a semimetal.[1] For 1-D semimetal the donor, e.g., TTF, gives some electrons to the acceptors, e.g., TCNQ. This gives rise to two partially occupied conduction bands.

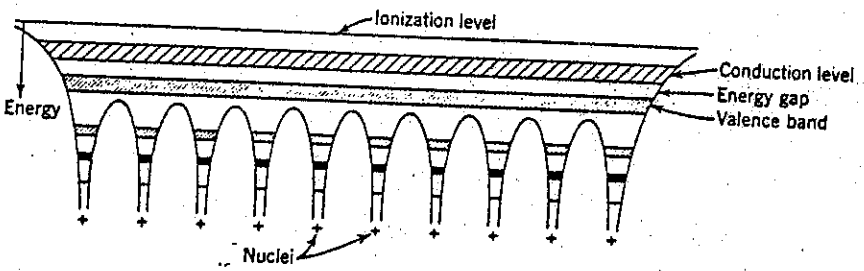


Fig. 1.2 Energy bands in a solid. The bands arise from the splitting of the energy levels of individual atoms (or molecules), as these are brought into close proximity, forming a solid. Electrons may move freely in the conduction band and positive holes, or electron vacancies, in the valence band.

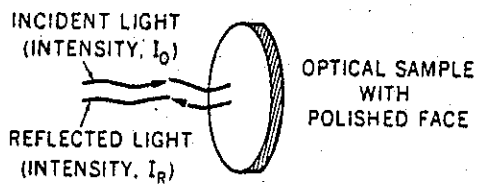


$$R \equiv \frac{I_R}{I_0}$$

Fig. 1. Features of reflectivity measurements at normal incidence used to determine the free-carrier electric-susceptibility mass in semiconductors.

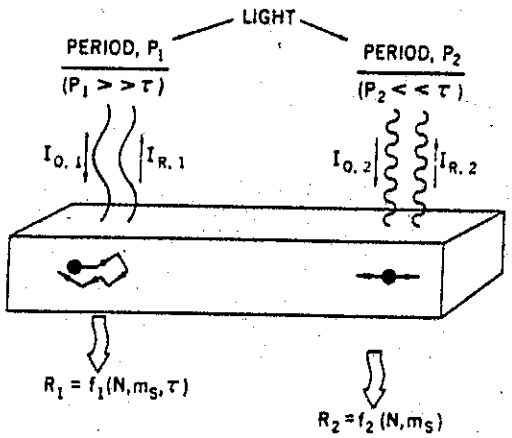


Fig. 2. Elementary phenomena involved in the interaction of light with free carriers. The dependence of the reflectivity $R$ upon the carrier concentration $N$, the effective mass $m_s$, and the average scattering time $\tau$ is expected to vary with the period or frequency of the light.

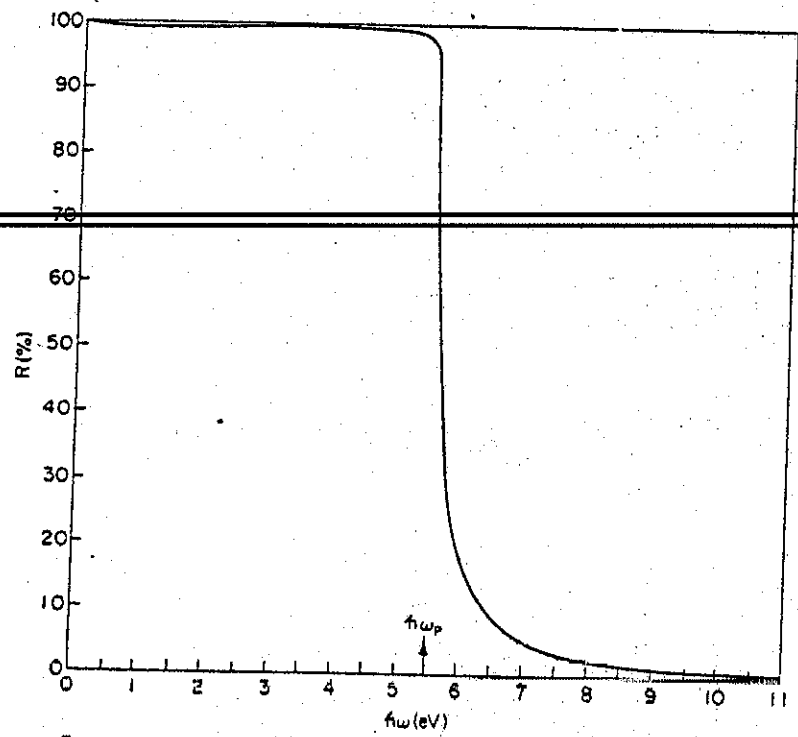


Spectral dependence of reflectivity for a free-electron metal.

Fig 3

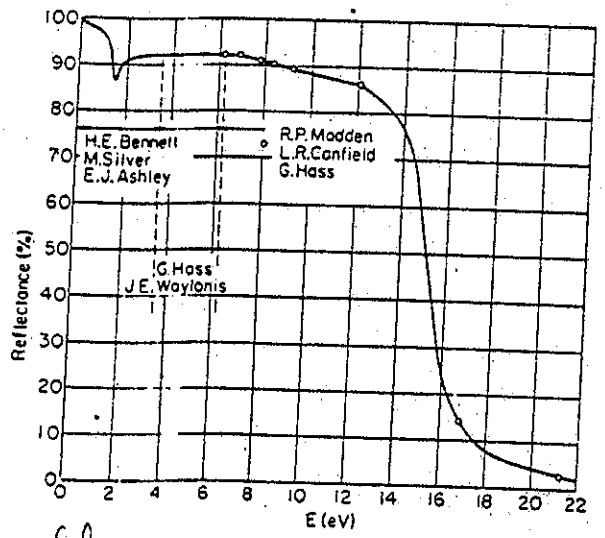


Fig 4 Reflectance of Al $\hbar\omega = 14{,}7$ ev → resonance de plasma

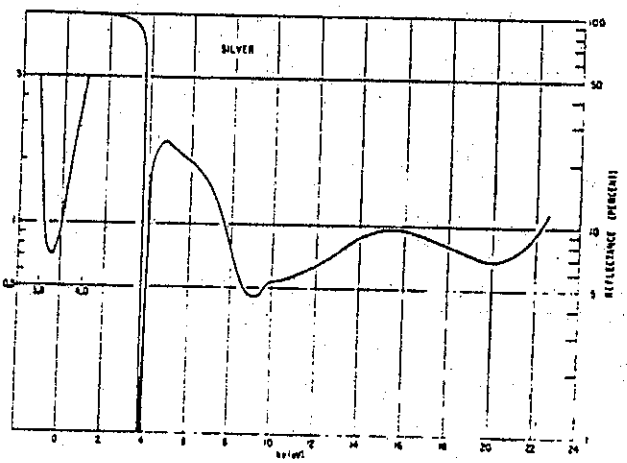


(a)

$\hbar\nu \to 4$ ev $\nu : 310$ n.m.

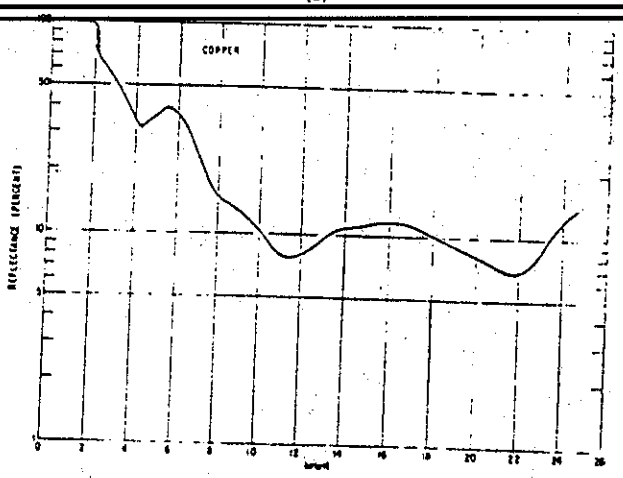


(b)

Fig 5 . Spectral dependence of the reflectance of Ag and Cu.

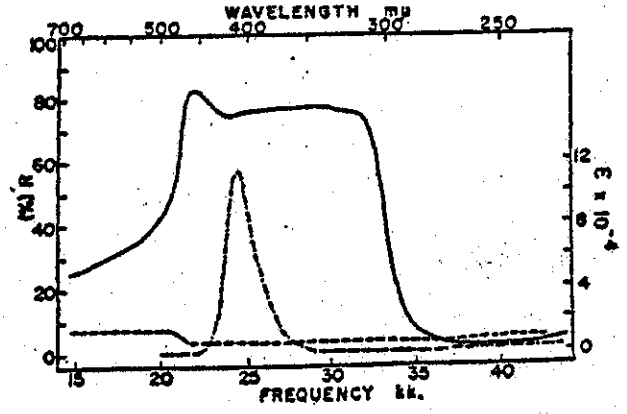


fig 6

FIG. 1. Crystal reflection spectra for face 1 of 1,5-bis-(dimethylamino)pentamethinium perchlorate obtained with light polarized along principal directions 1 (——) and 2 (– – –); and the absorption spectrum of a water solution of the same compound (—·—·).

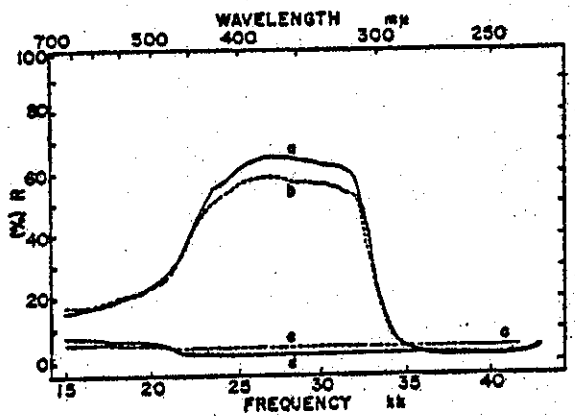


(7)

FIG. 4. Crystal reflection spectra of faces 2 (——) and 3 (– – –) of 1,5-bis-(dimethylamino)pentamethinium perchlorate. For each face, the curve which shows the metallic reflection peak (*a*; *b*) is that obtained with light polarized along principal direction 1, and the relatively structureless curve (*c*; *d*) is that obtained with light polarized along principal direction 2.

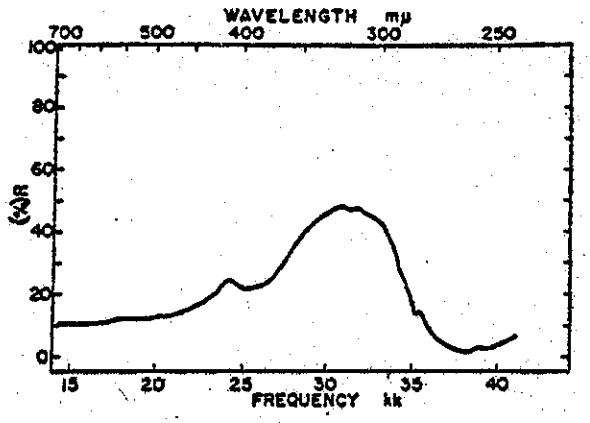


FIG. 5. Crystal reflection spectrum for one face of 5-*N*-methylanilino-2,4-pentadienal obtained with light polarized along one of the principal directions.

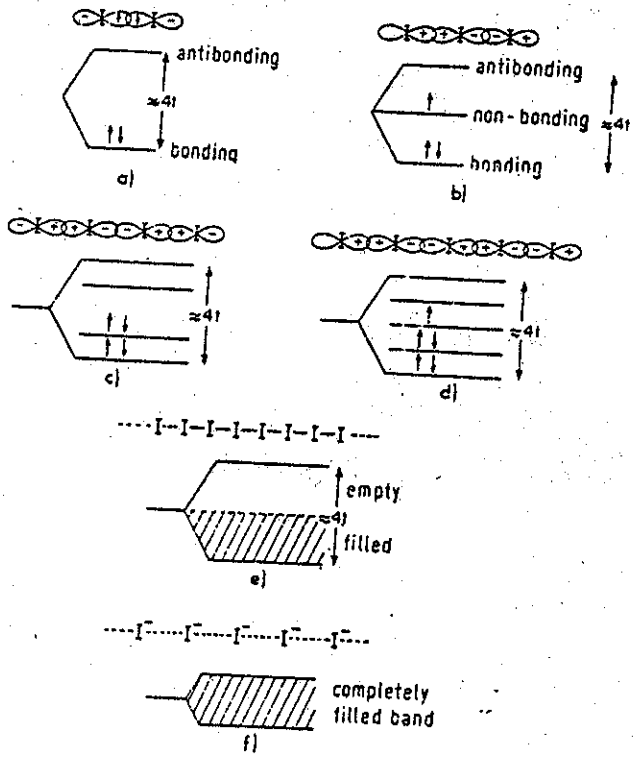


Fig. 1. LCAO-MO energy level scheme for: a) $I_2$ molecule; b) $I_3$; c) $I_4$; d) $I_5$; e) $I_\infty$; and f) $(I^-)_\infty$. Notice that separation between lowest filled and highest empty MO (*ca.* 4 *t*) is roughly independent of the number of atoms in the chain.

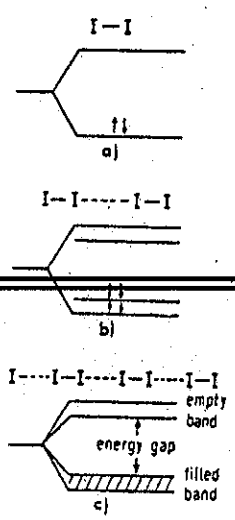


Fig. 2. LCAO-MO energy level scheme for a chain of $I_2$ molecules a) $I_2$; b) $(I_2)_2$; c) $(I_2)_\infty$. Dimerization produces an energy gap not present in Fig. 1c.

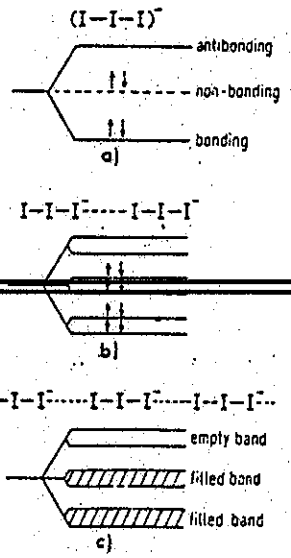


Fig. 3. LCAO-MO energy level scheme for a chain of $I_3^-$ ions. a) $I_3^-$; b) $(I_3^-)_2$; and c) $(I_3^-)_\infty$.

table II

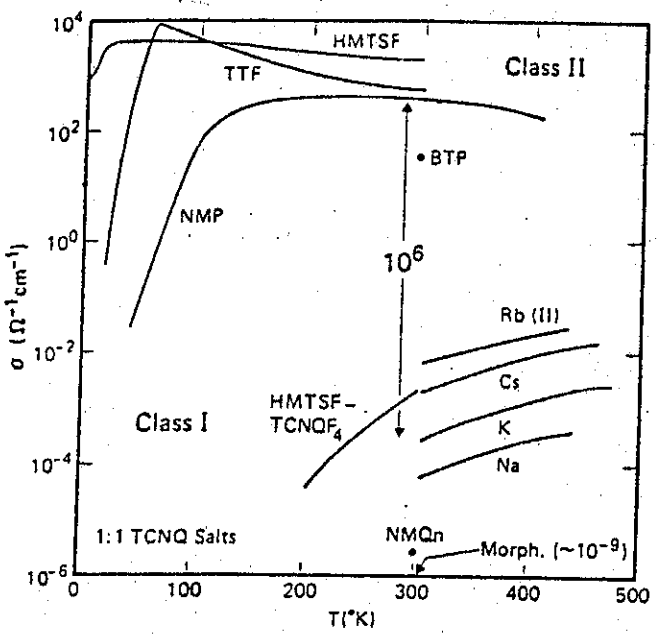


table I

Figure 1. The single-crystal dc conductivity along the stacking axis for a number of 1:1 TCNQ salts, showing the large differences in conductivity between the metals of class II and the insulators of class I. For the meaning of abbreviations, see Tables I and II

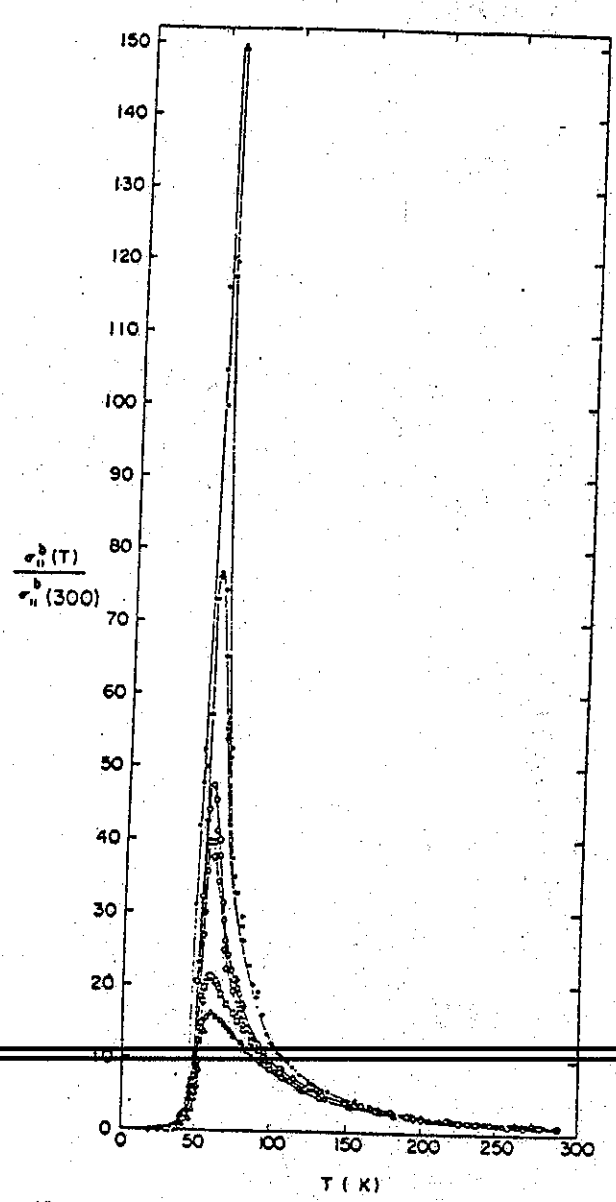


FIG. 43. — *Normalized dc conductivity as a function of temperature for different single crystals of TTF—TCNQ. These results have been shown to be intrinsic. Peak reaches normalized values of 17 to 150. Value of 500 has been reported earlier* [26] *(reproduced with permission of* [16]*).*

• BTP : 4,4'-bithiopyrylium

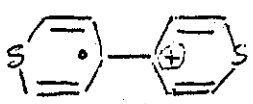

19,8 mm → 50 K
x mm → $\frac{50}{19,8}$ . x K

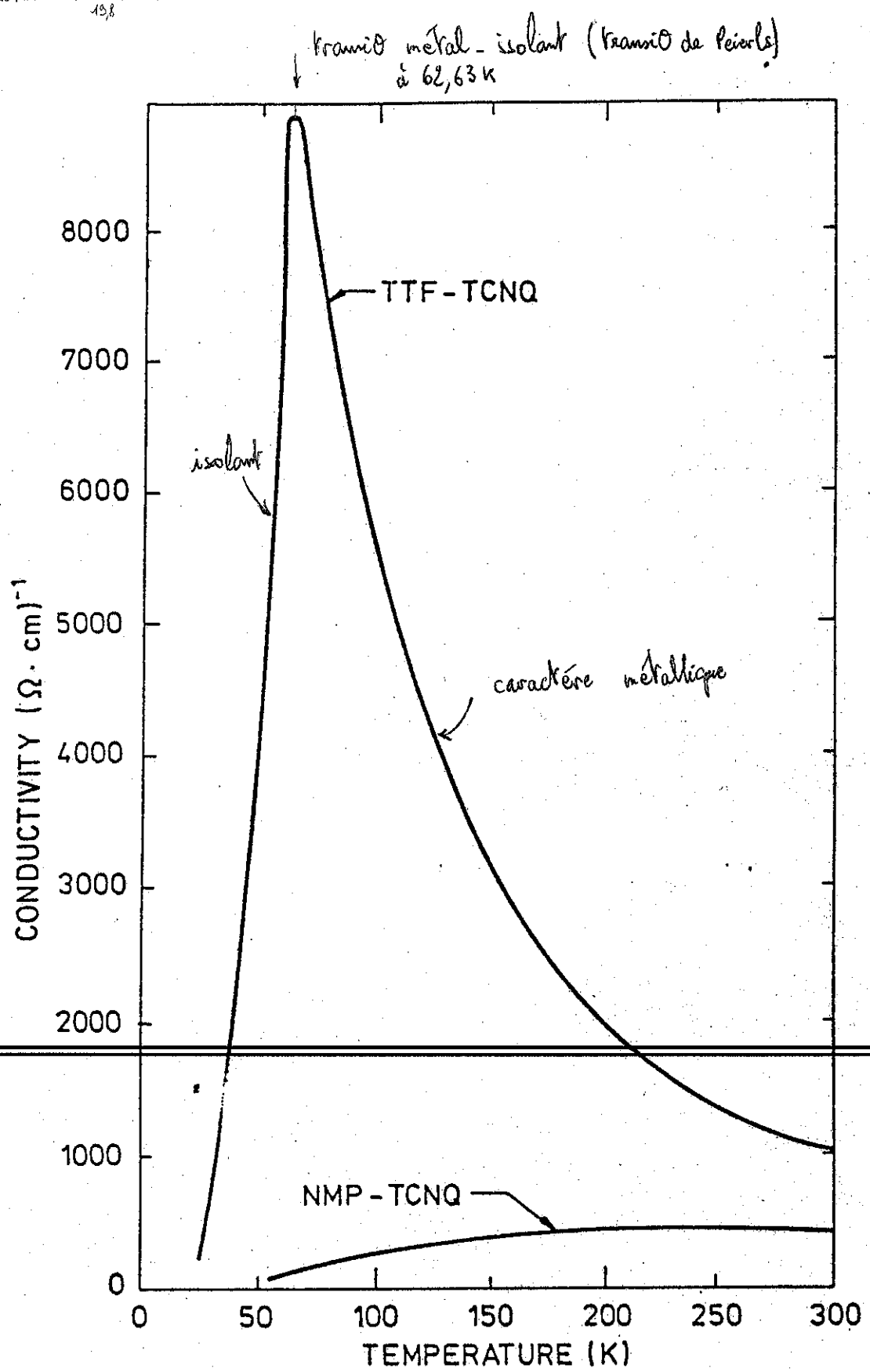


Absolute conductivities of representative single crystals of TTF-TCNQ and NMP-TCNQ recorded in the most conductive crystallographic directions.

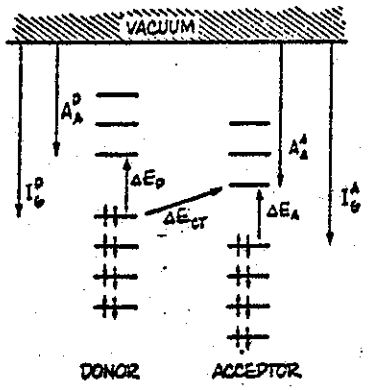


Energy level diagram for weakly interacting closed-shell components of a $\pi$-complex emphasizing energy levels of components.

(1)

Donor ionisation potentials and electrochemical half-wave potentials.

| | IP (eV) | $E_{\frac{1}{2}}^{1*}$ | $E_{\frac{1}{2}}^{2}$ |
|---|---|---|---|
| TTF | 6.83[24)] | 0.27 | 0.64 |
| TMTTF | 6.42[24)] | 0.24 | 0.61 |
| HMTTF | - | 0.27 | 0.60 |
| TSF | 7.21[§25)] | 0.42 | 0.70 |
| TMTSF | 6.58[24)] | 0.35 | 0.59 |
| HMTSF | - | 0.35[‡] | 0.59 |
| DEDMTSF | 6.45 | 0.35 | 0.59 |

~~Acceptor electron affinities and electrochemical~~ half-wave potentials.

| | EA (eV) | $E_{\frac{1}{2}}^{1*}$ | $E_{\frac{1}{2}}^{2}$ |
|---|---|---|---|
| TCNQ | 2.8 ± 0.1[28)] | 0.19 | -0.35 |
| MTCNQ | - | 0.17 | -0.34 |
| DMTCNQ | - | 0.11 | -0.35 |
| DETCNQ | - | 0.12 | -0.37 |

* Volts vs. SCE at Pt-button electrode in $CH_3CN/n\text{-}Bu_4NBF_4$ (0.1M)

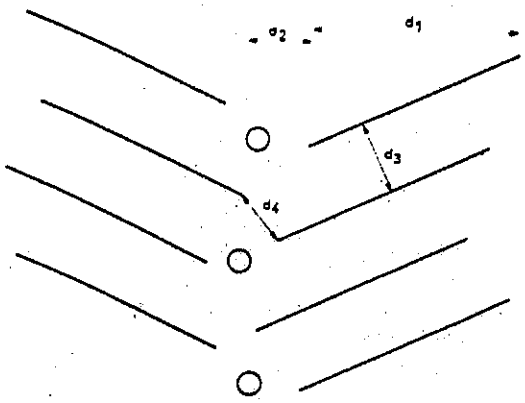


FIG. 22. — *Schematic stack of RIS with small counter-ions. This figure is taken from the crystalline structure of* $Cs_2 - TCNQ_3$ *(projection 100). Stacks are parallel to b axis (after* [29]).

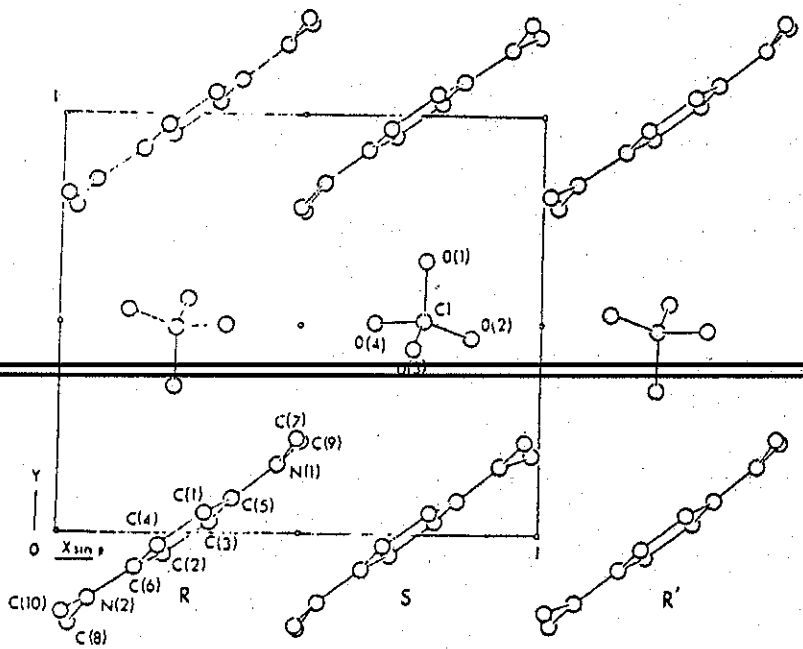


FIG. 6. — *Crystalline structure of 1 : 1 RIS TMPD —* $ClO_4$ *at 77 K (projection 001). Stacks are parallel to a axis (reproduced with permission of* [52]).

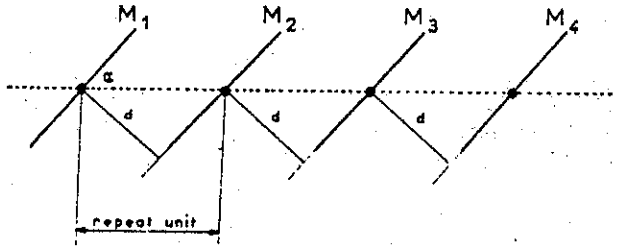


FIG. 17. — *Schematic representation of molecules* $M_i$ *in a regular chain.*

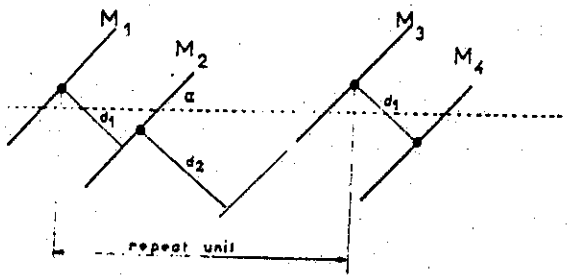


FIG. 18. — *Schematic representation of molecules* $M_i$ *in a diadic chain.*

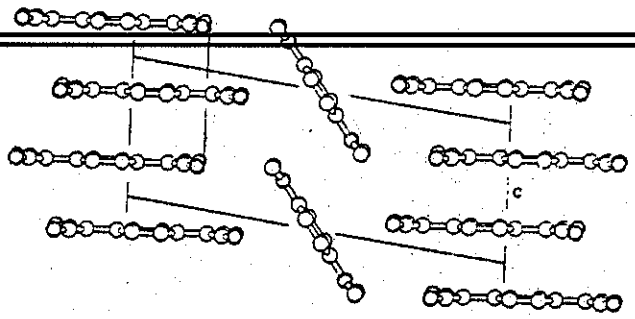


FIG. 3. — *Crystalline structure of 1 : 2 CTC TMPD — $TCNQ_2$ (projection 100). Stacks are parallel to c axis*

9

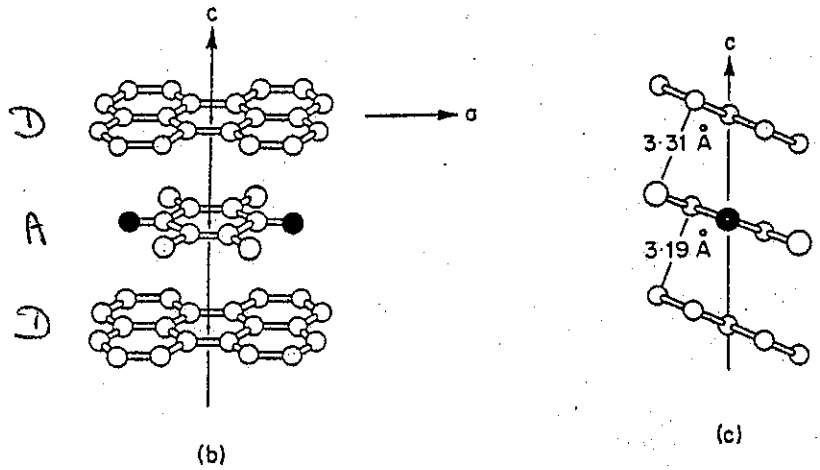


(b) (c)

Perylene:fluoranil. Crystal structure

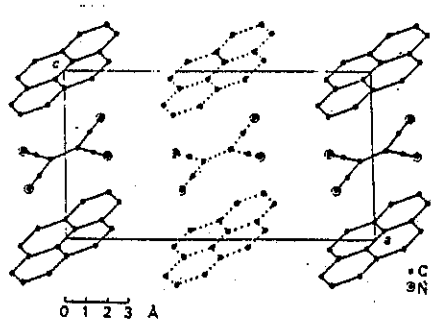


— Crystalline structure of 1 : 1 CTC Pyrene-TCNE

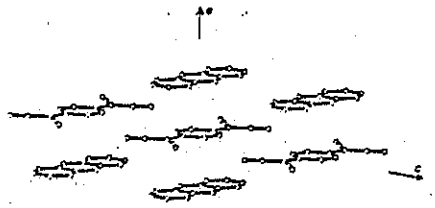

— Crystalline structure of 1 : 1 CTC DPDO — TCNQ (projection 010). Stacks are parallel to a axis

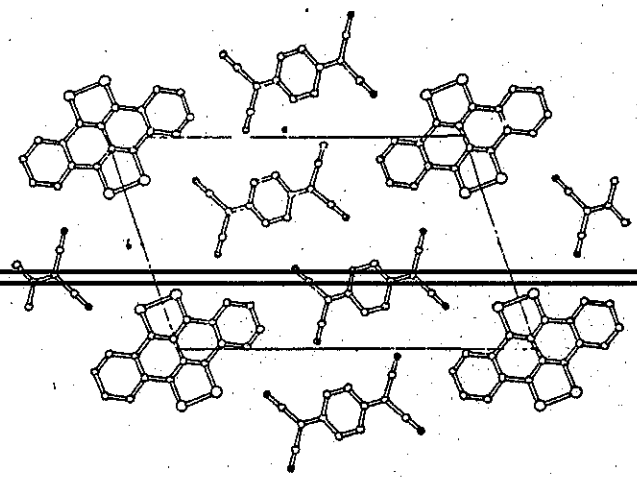

— Crystalline structure of 1 : 2 CTC TTT — $TCNQ_2$ (projection 001). Stacks are parallel to c axis

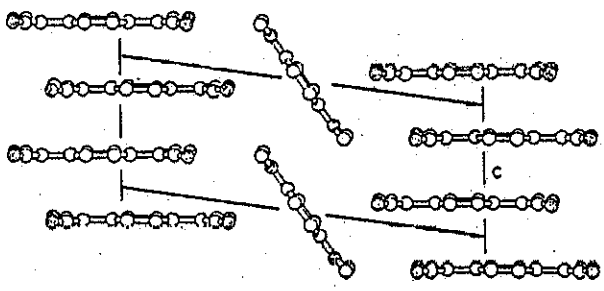


TMPD:$(TCNQ)_2$.

The structure viewed along the normal to the plane (110).

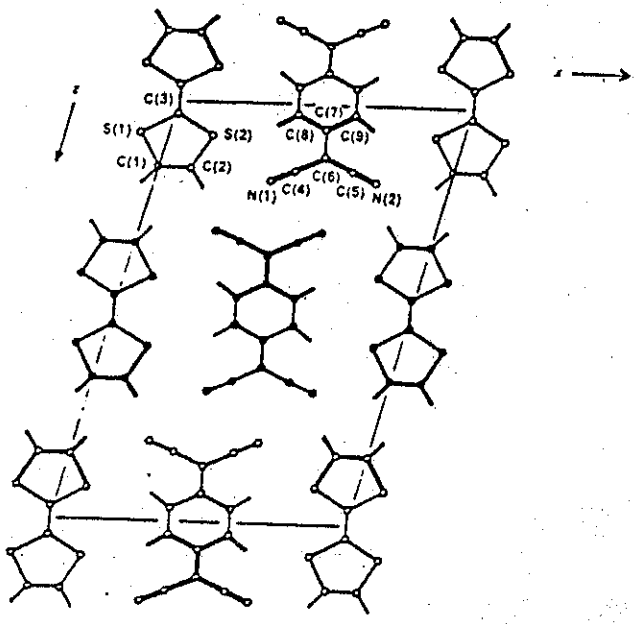


FIG. 15. — *Crystalline structure of 1 : 1 CTC TTF — TCNQ (projection 010). Stacks are parallel to b axis*

TABLE IX

*Overlap ($\delta x$, $\delta y$) and distance ($d$) between two consecutive molecules in regular chains* (fig. 21). *The distances ($d'$) between counter-ions are taken in the stack direction. The CTC TTF — TCNQ and TTT — $TCNQ_2$ appear twice: one for the TCNQ chains and once for the TTF or TTT chains. Systems are listed with increasing distance ($d$). For the meaning of $\delta x$ and $\delta y$ see text and figure 19.*

| SYSTEM | d Å | δx Å | δy Å | d' Å counter-ions | REF. |
|---|---|---|---|---|---|
| TTF-TCNQ | 3.17 | 0 | 2.15 | CTC | 14 |
| TTT-$TCNQ_2$ | 3.18 | | | CTC | 74 |
| Q-$TCNQ_2$ | 3.22 | 0 | 2.15 | 3.50 | 40 |
| Ac-$TCNQ_2$ | 3.25 | 0.09 | 2.08 | 3.42 | 42 |
| NMP-TCNQ | 3.26 | 0 | 2.02 | 3.36 | 43 |
| TMPD-I | 3.38 | 0 | ~ 4.80 | 5.92 | 50 |
| Cr complex-TCNQ | 3.42 | 1.08 | 0.06 | non planar counter-ion | 47 |
| Rb-TCNQ(II) | 3.43 | ~ 0 | 1.92 | 3.39 | 28 |
| TTF-TCNQ | 3.47 | 0 | 1.43 | CTC | 14 |
| K-CA | 3.47 | 1.95 | 0.15 | 3.71 | 61 |
| TTT-$TCNQ_2$ | 3.52 | | | CTC | 74 |
| TMPD-$ClO_4$ | 3.55 | ~ 0 | ~ 5.0 | 5.96 | 51 |

TABLE XII

*Some typical Van der Waals distances* ([76], p. 260). (1) *This value is the half of the intermolecular distance between two consecutive TCNQ molecules in a stack in neutral TCNQ crystals* [75].

Van der Waals Radii of atoms

| | |
|---|---|
| H | 1.2 Å |
| N | 1.5 Å |
| O | 1.40 Å |
| S | 1.85 Å |
| Cl | 1.80 Å |
| I | 2.15 Å |

Radius of methyl group, $CH_3$, 2.0 Å

Half thickness of aromatic molecule, 1.70 Å

Half thickness of TCNQ, 1.72 Å (1)

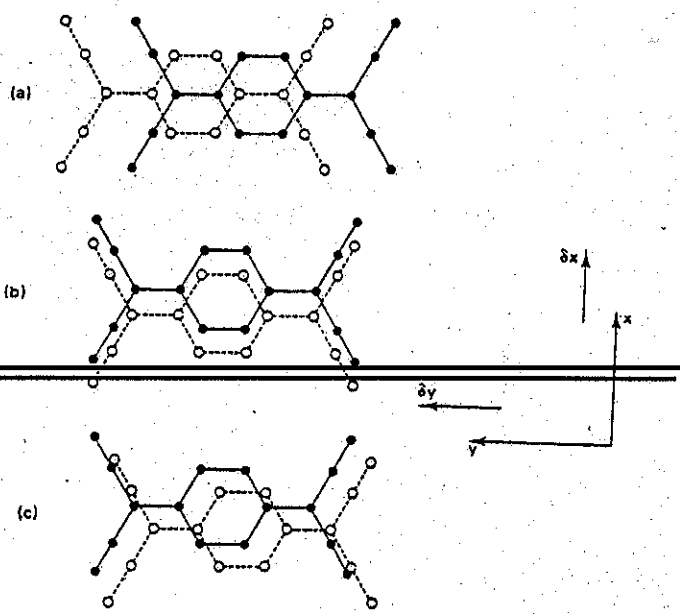


FIG. 19. — *Typical overlaps for consecutive molecules in stacks of TCNQ.*

*a*) Ring-external bond overlap $d(AB) = 3.25$ Å; *b*) Ring-ring overlap $d(BB') = 3.24$ Å; *c*) Unusual overlap $d(BB') = 3.43$ Å. *a*) and *b*) have been obtained by [35] on (Morpholinium)$_2$-$TCNQ_3$ and *c*) by [41] on NPQ — $TCNQ_2$.

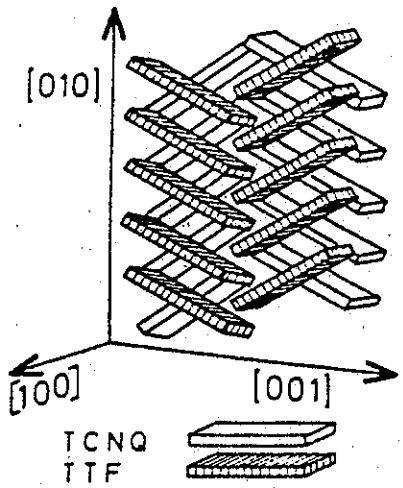


Schematic representation of the TTF-TCNQ structure. Note that the molecular plane is not perpendicular to the stacking axis b ([010]) but tilted around the a axis ([100]), that there are two identical molecules with opposite tilts for one repeat unit along the c direction ([001]), and that there are alternatively TCNQ and TTF stacks in a direction.

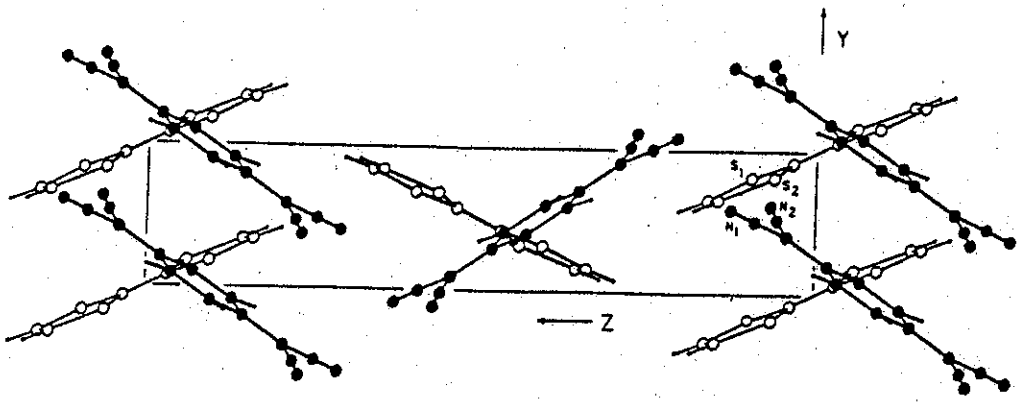


- Crystal structure of TTF-TCNQ projected along the a-axis.

TABLE I

Electronically Significant Interchain Contacts

| | Contact | Number | Distance, A | van der Waals Distance, A |
|---|---|---|---|---|
| TTF-TCNQ | S···N (a) | 2 | 3.20 | 3.35 |
| | S···N (a) | 2 | 3.25 | 3.35 |
| | C···N (a) | 2 | 3.29 | 3.10 |
| TMTTF-TCNQ | S···N | 2 | 3.45 | 3.35 |
| | S···S | 2 | 3.66 | 3.70 |
| TMTSF-TCNQ | Se···N | 2 | 3.36 | 3.50 |
| | Se···Se | 2 | 4.00 | 4.00 |
| HMTSF-TCNQ | Se···N | 4 | 3.10 | 3.50 |

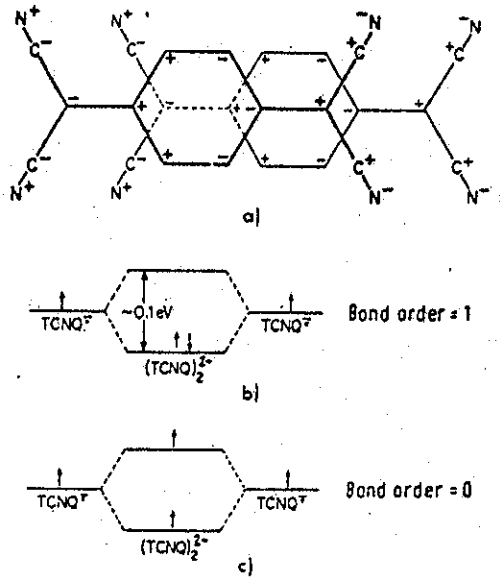


Fig. 5. a) Preferred stacking arrangement of TCNQ ions. Positive and negative signs of the $b_{2g}$-$p_\pi$ orbitals above the plane of each molecule are indicated, b) LCAO-MO energy scheme for $(TCNQ^-)_2$ assuming that Coulomb repulsion between electrons is small. c) Same as (b) but with large Coulomb repulsion.

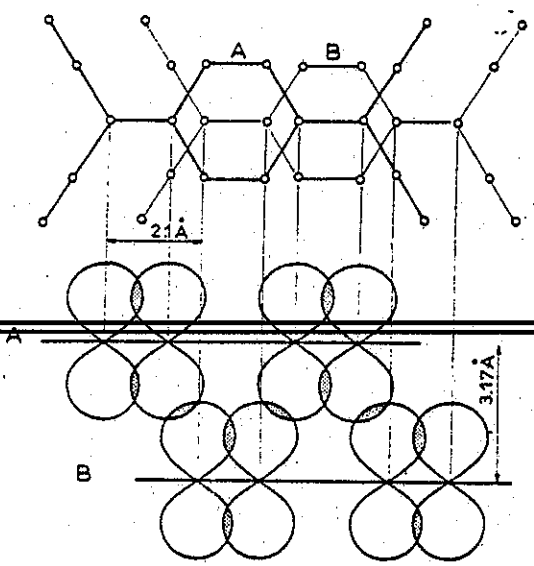


FIG. 25. — *Schematic overlap of the $p_z$ orbitals of carbon atoms between two consecutive TCNQ in the geometry of the stack of TTF — TCNQ.*

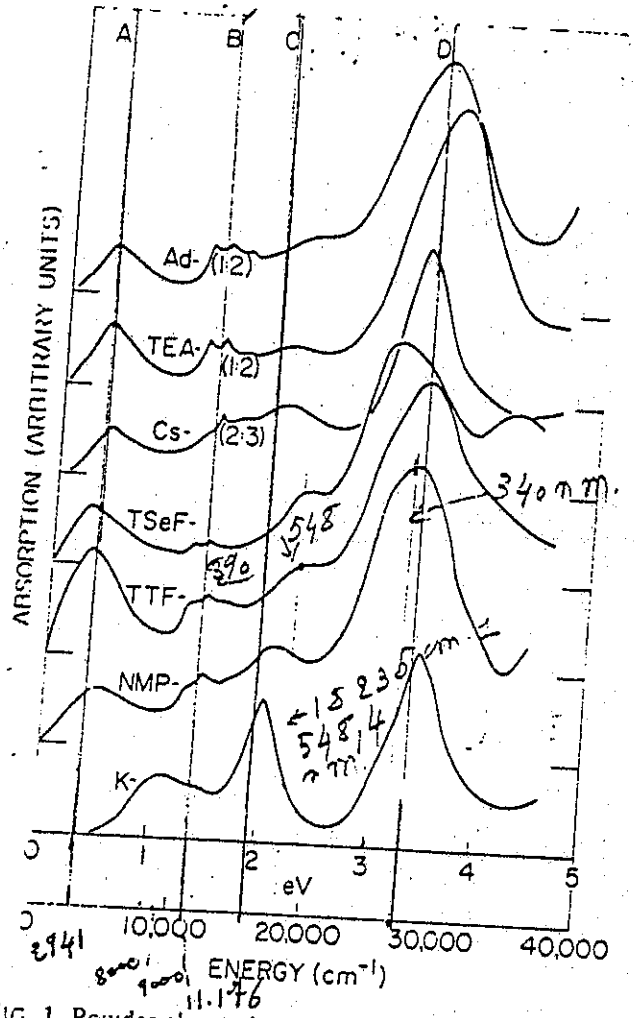


FIG. 1. Powder absorption spectra measured on KBr disks and normalized per mole TCNQ.

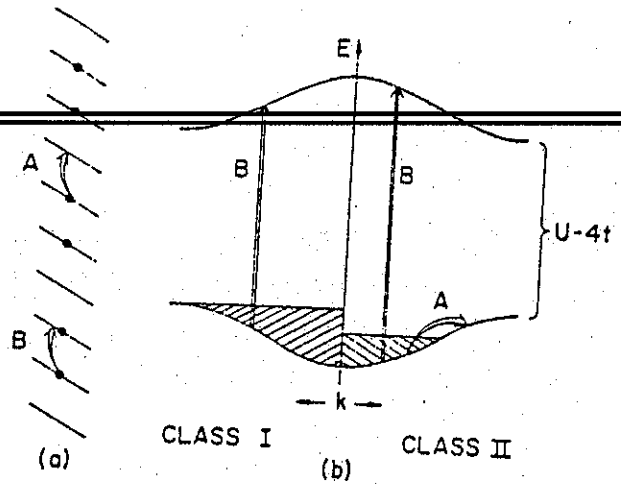


FIG. 2.(a) Localization of electrons (·) on TCNQ molecules (/) in $Cs_2TCNQ_3$; (b) excitations from filled (left side) and partially filled (right side) Hubbard-like bands (schematic).

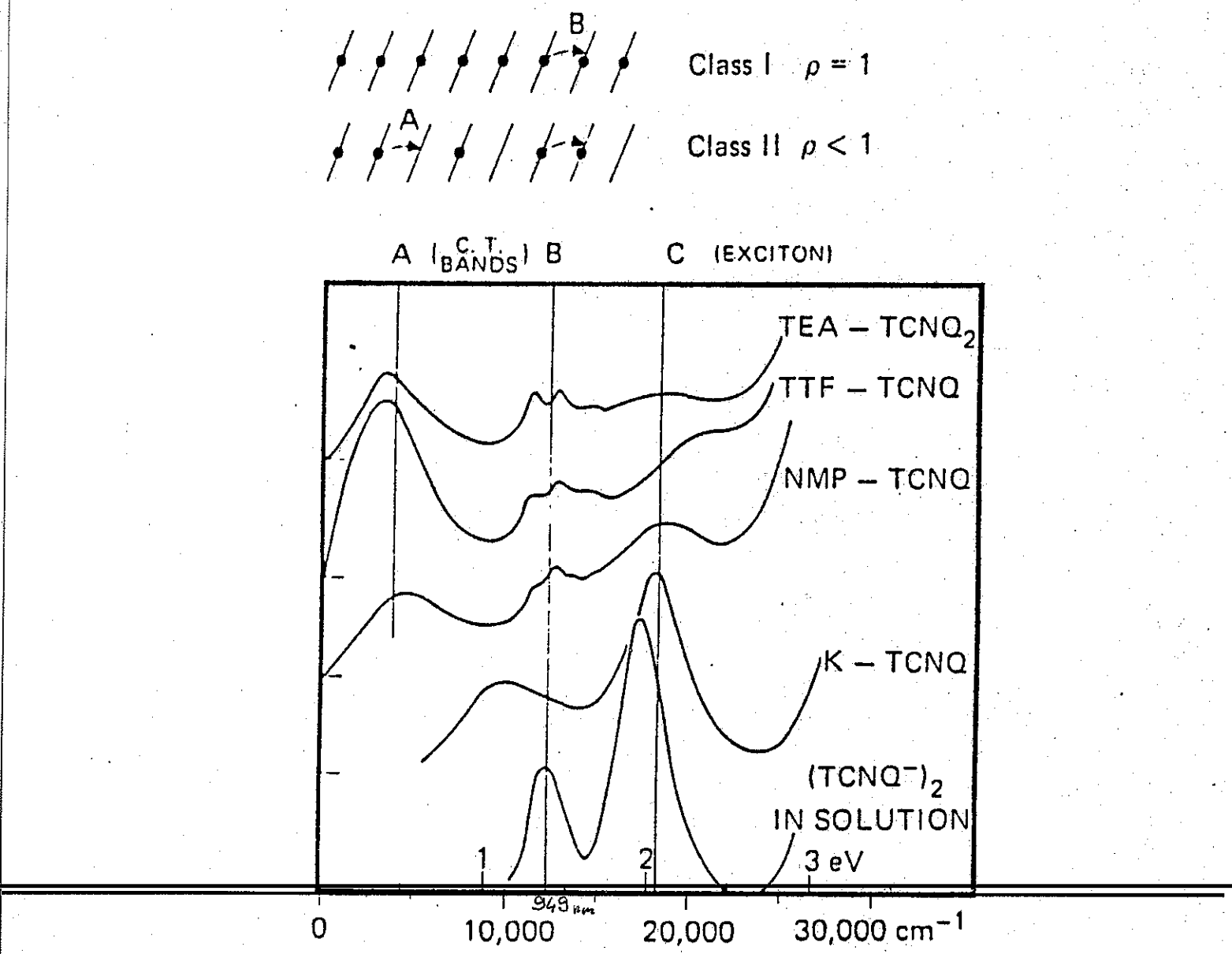


(Top) Schematic diagram, illustrating the differences between the electronic structures proposed for the TCNQ stacks in class I and II salts. (Bottom) Powder absorption spectra for a number of representative TCNQ salts

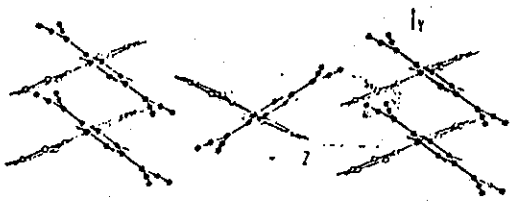

Fig. 3. Projection of crystal structure for TTF-TCNQ *(14)* along the *x*-axis [159]. Separate stacks of TTF and TCNQ occur along the *y*-axis but along *x* the donor and acceptor are at an angle of 58.5°.

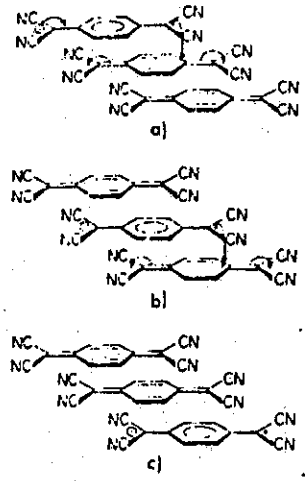

Fig. 4. Stacking arrangement for mixed-valence TCNQ ions: a) $TCNQ^{+}$ with aromatic sextet transfers charge to neutral TCNQ with no aromaticity resulting in b) and then again in c). Aromaticity migrates down the TCNQ stack along with the unpaired electron.

(donné I) Table I (voir fig 1 p 4)

Cations of Class I TCNQ Salts with Their 300 K Powder Conductivities and Peak Reduction Potentials, $E_p$

| | | Ref. | $\sigma(\Omega^{-1}cm^{-1})$ | $E_p$(eV) |
|---|---|---|---|---|
| $Na^{+}$ | | [5,40 50-52] | $3 \times 10^{-5}$ | -3.0 |
| ($Li^{+}$,$K^{+}$,$Cs^{+}$,$Rb^{+}$) | | | ($10^{-4}$-$10^{-6}$) | |
| triethylammonium (TEA) | 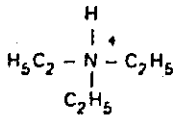 | [5,25] | $10^{-9}$ | -2.8 |
| (ammonium $NH_4^{+}$) | | [5,25] | ($2 \times 10^{-5}$) | |
| morpholinium (Morph) | 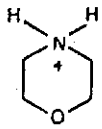 | [5,25,49] | $10^{-9}$ | -2.8 |
| N-methylpyridinium (NMPy) | 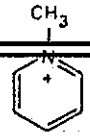 | [5] | $10^{-5}$ | -1.28 |
| (pyridinium) | | [5] | ($10^{-6}$) | |
| (4-cyano-NMPy) | | [5] | ($10^{-6}$) | |
| N-methylpyrazinium (NMPyz) | 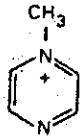 | [24] | $3 \times 10^{-8}$ | -0.73 |
| N-methylquinolinium (NMQn) | 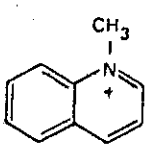 | [5,25] | $10^{-7}$ | -0.86 |
| (4-cyano-NMQn) | | [5] | ($10^{-8}$) | |
| (8-hydroxy-NMQn) | | [6] | ($2 \times 10^{-7}$) | |
| N-methylacridinium (NMAd) | 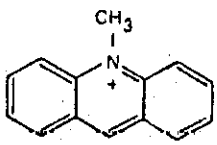 | [24] | $2 \times 10^{-5}$ | 0.41 |

Table II (classe II)

Cations of Class II TCNQ Salts with Their 300 K Powder Conductivities and Peak Reduction Potentials, $E_p$ (after ref 22)

| | | Reference | $\sigma$ ($\Omega^{-1}cm^{-1}$) | $E_p$(eV) |
|---|---|---|---|---|
| N-methylphenazinium [NMP] | 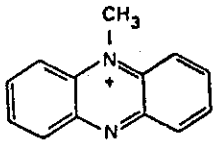 | [6,24,25,48] | 2 | -0.11 |
| tetrathiafulvalinium [TTF] | 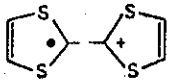 | [10,11,53] | 10 | + 0.31 |
| tetraselenafulvalinium [TSeF] | | [12,42] | (18) | (+0.44) |
| hexamethylene – TSeF [HMTSF] | 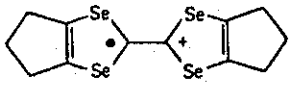 | [14,54] | 25 | +0.41 |
| Δ 4, 4' bithiopyranium [BTP] | 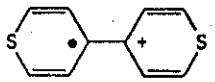 | [31] | 1 | +0.08 |

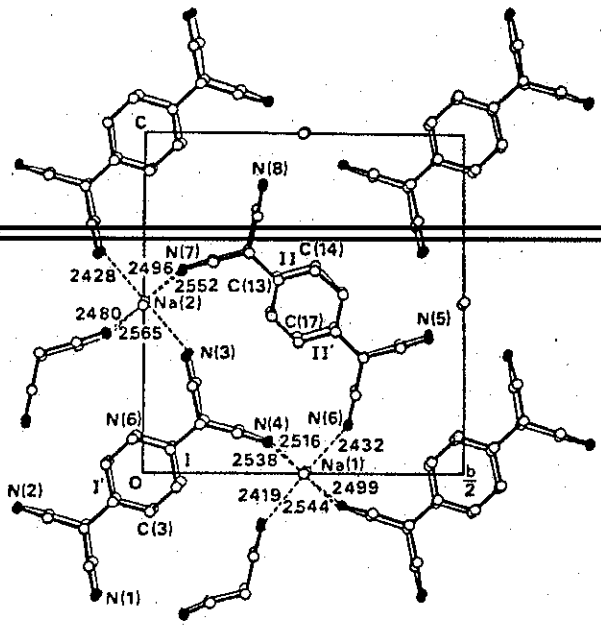


FIG. 10. — *Crystalline structure of 1 : 1 RIS Na — TCNQ (projection 100). Both crystallographically inequivalent TCNQ (I and II) are stacked parallel to a axis*

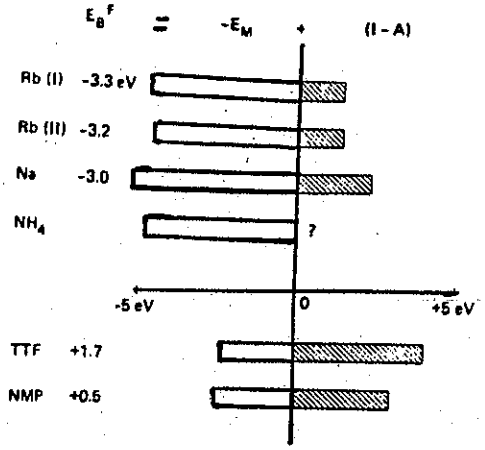


A graphical representation of the Madelung energies and values of (I–A), illustrating the differences in both of these quantities between salts of class I and those of class II

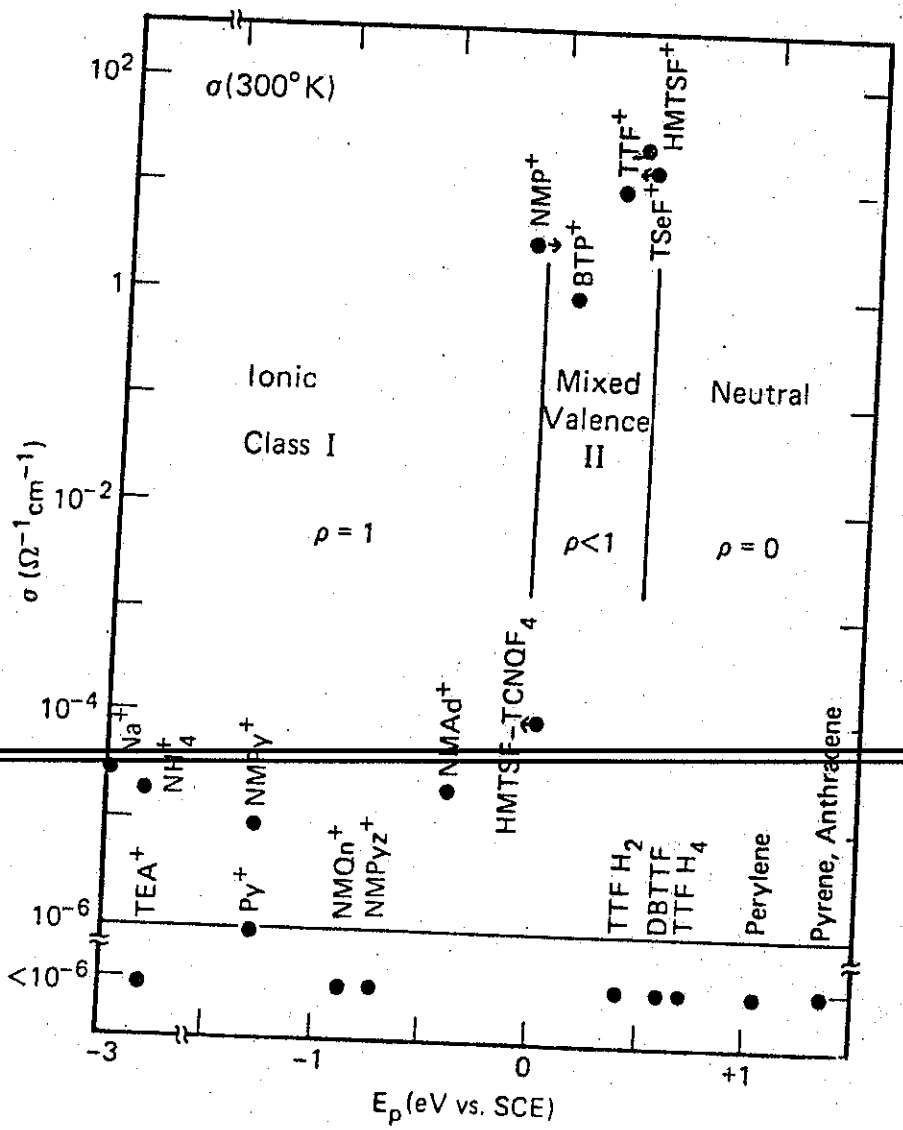


The conductivity of the known 1:1 TCNQ salts plotted vs. the reduction potential of the cation.

Arrows represent the direction of the effect of Madelung energy.

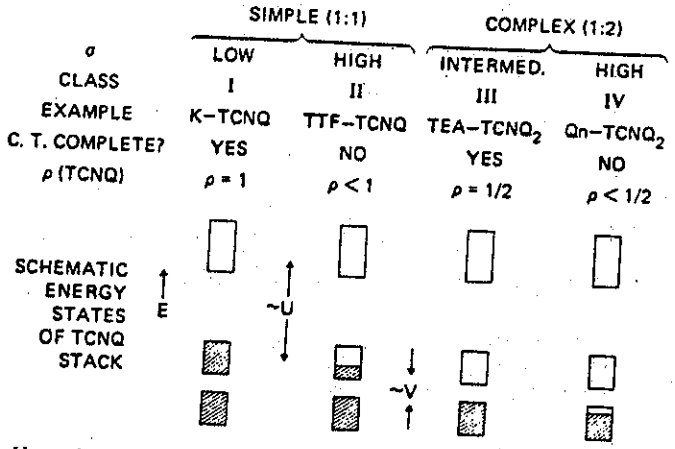


FIGURE 3. How the TCNQ salts are classified on the basis of the magnitude of their conductivity and are interpreted in terms of different values of $\rho$, the average number of unpaired electrons per molecule.

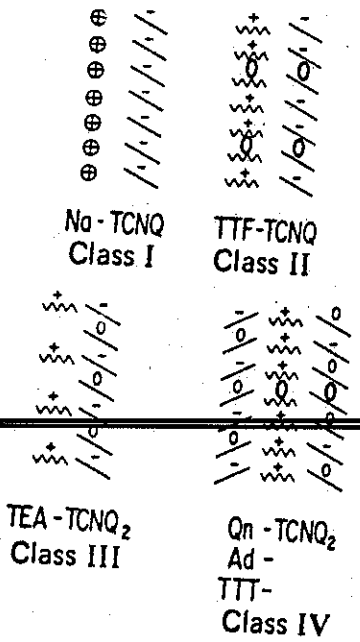


FIGURE 10. Schematic diagram of the stacks and charges in representative examples of each of the four classes.

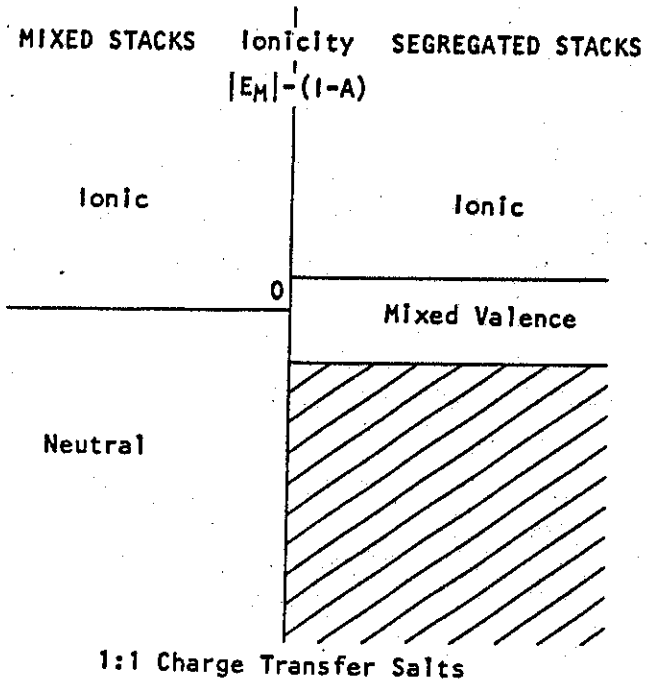


Fig. 2. The phase diagram showing the four different phases found for 1:1 charge transfer systems and showing how these phases are determined by the stacking and the strength of ionicity (the degree of charge transfer).

TABLE 2

THE CATIONS OF COMPLEX TCNQ SALTS, DIVIDED INTO CLASS III AND IV

Class III Cations
(1:2 salts unless noted)

$Cs^{+}$[2,39,63] (2:3)

triethylammonium[2,66] [TEA]

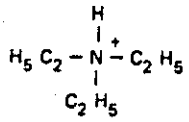

N-propylquinolinium[2,64] [NPQn]
(4-cyano-N-methyl Qn [CNNMQn])

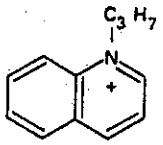

methyl-triphenylarsonium[38,65] [M $\phi_3$ As]
(Me $\phi_3$ P)[65]

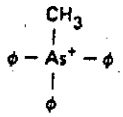

N,N,N',N' -tetramethyl-p-phenylenediamine[74] [TMPD]

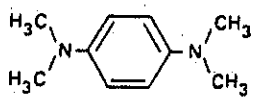

3,3-diethylthiazolinocarbocyaninium[3] [$Et_2$ Tz CC]
(intermediate conductivity form)

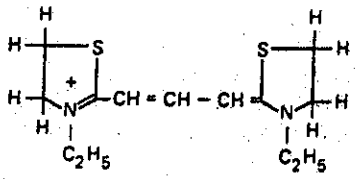

4-4' Bipyridinium[16,17]

1,2-di (N-ethyl-4-pyridinium) ethylene[87] [DEPE] (1:4)
(form II)

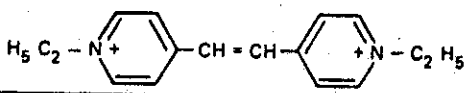

TABLE 2 (*Continued*)

Class IV Cations
(1:2 salts unless noted)

quinolinium[3,37,69] [Qn]
(N-methyl Qn, phase A)

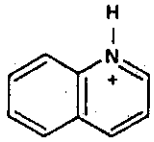

acridinium[3,37,70] [Ad]
(N-methyl Ad)

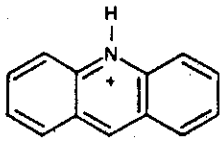

tetrathiotetracene[36,71] [TTT]

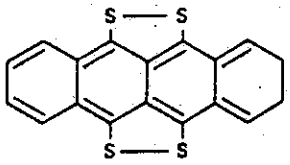

3,3-diethylthiazolinocarbocyaninium[3] [$Et_2$ Tz CC]
(high conductivity form)

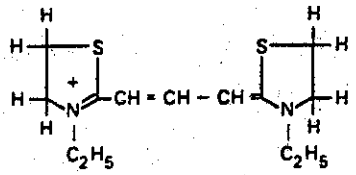

2-2' Bipyridinium[16,17]

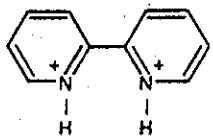

1,2-di (N-ethyl-4-pyridinium) ethylene[87] [DEPE] (1:4)
(form I)

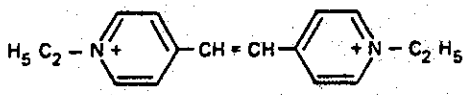

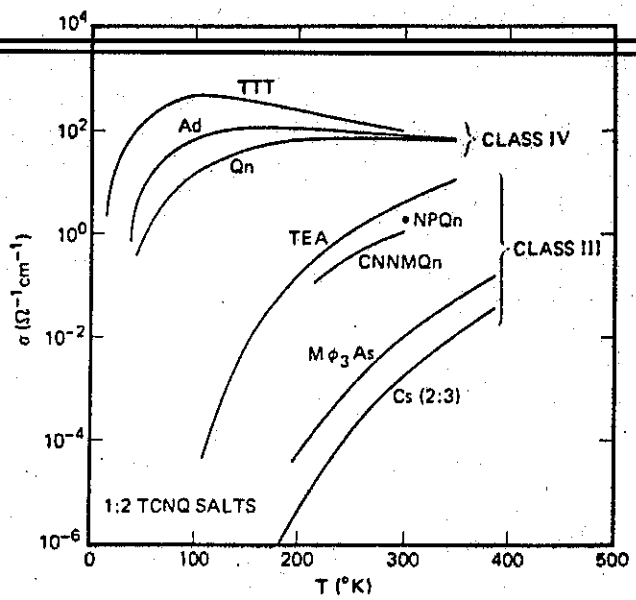


FIGURE 2. The temperature dependence of the conductivity of a number of complex TCNQ salts, illustrating how they can be divided into two classes (III and IV). (For meaning of abbreviations, see TABLE 2.)

| | |
|---|---|
| A 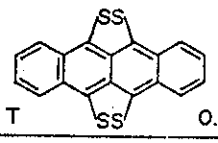 TTT 0.24 | B 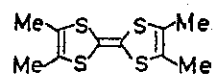 TMTTF 0.27 |
| C 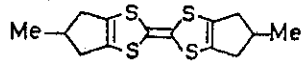 0.30 | D 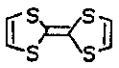 TTF 0.31 |
| E 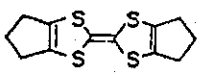 HMTTF 0.33 | F 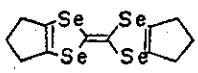 HMTSF 0.41 |
| G 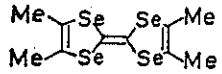 TMTSF 0.44 | H 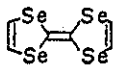 TSF 0.44 |
| I 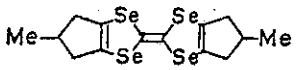 0.48 | J 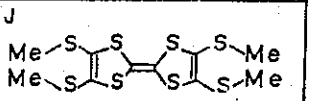 0.50 |
| K 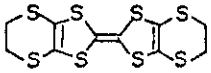 0.53 | L 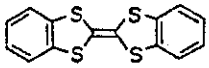 DBTTF 0.53 |

Fig. 1. Electron donors with corresponding electrochemical half-wave potentials.

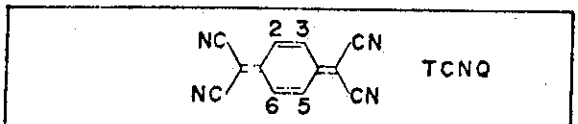


| | | |
|---|---|---|
| a 2,5-$(CN)_2$ 0.65 | b $F_4$ 0.53 | c 2,5-$(Br)_2$ 0.41 |
| d 2,5-$(Cl)_2$ 0.41 | e 2,5-$(I)_2$ 0.35 | f 2,5-$(F)_2$ 0.33 |
| g Br 0.29 | h Cl 0.29 | i F 0.26 |
| j 2,5-Cl,Me 0.26 | k 2,5-Br, Me 0.26 | l 2,5-I,Me 0.25 |
| m TCNQ 0.14 | n Me 0.12 | o 2,5-$(^{i}Pro)_2$ 0.12 |
| p 2,5-$(Et)_2$ 0.11 | q 2,5-$(Me)_2$ 0.10 | r 2,5-OEt, SMe 0.08 |
| s OMe 0.07 | t 2,5-$(OMe)_2$ -0.01 | u 2,5-OMe,OEt -0.02 |

Fig. 2. Electron acceptors with corresponding electrochemical half-wave potentials.

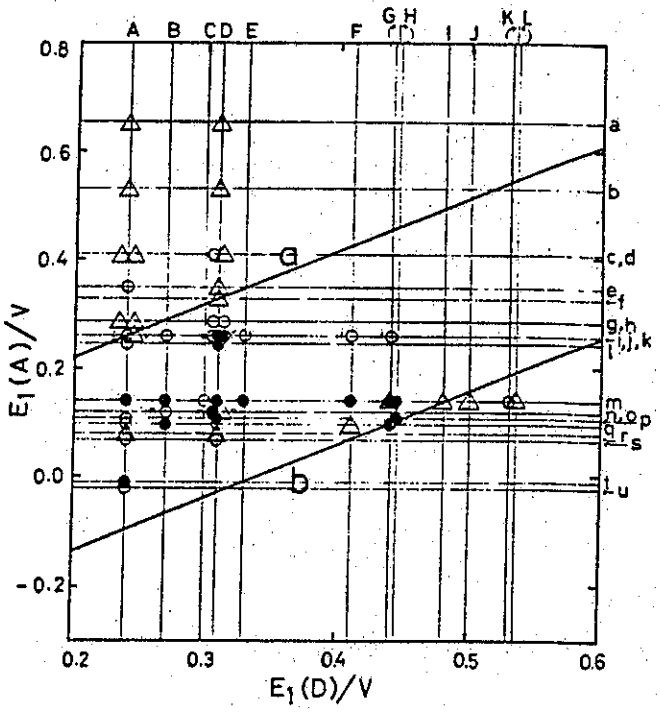


Fig. 3. Conductivity of complexes plotted as $E_1$ (A) *vs.* $E_1$ (D).
△ = insulators or semiconductors; ○ = highly conducting in compaction studies; ● = "organic metals."